Tailoring perpendicular magnetic anisotropy in ultrathin Co/Pt multilayers coupled to NiO

H. Ouyang,[1] Y.-H. Han,[1] S.-C. Lo,[2] C.-H. Su,[3] Y.-R. Shiu,[3] K.-W. Lin,[3] R. D. Desautels,[4] and J. van Lierop[4]
[1]*Department of Materials Science and Engineering, National Tsing Hua University, Hsinchu, Taiwan 300, Republic of China*
[2]*Material and Chemical Research Laboratories and Nanotechnology Research Center, Industrial Technology Research Institute, Hsinchu, Taiwan 310, Republic of China*
[3]*Department of Materials Science and Engineering, National Chung Hsing University, Taichung, Taiwan 402, Republic of China*
[4]*Department of Physics and Astronomy, University of Manitoba, Winnipeg, Manitoba, Canada R3T 2N2*
(Received 10 May 2010; published 7 June 2010)

The nanomagnetism of ultrathin Co/Pt multilayer films is set largely by the microstructure and composition of the interface. To examine these finite-size effects on the Co/Pt magnetism, we have made different Co thickness multilayer films using an ion-beam deposition method with controlled ion energies via an End-Hall voltage (V_{EH}), and deposited a layer of NiO to examine the nature of the magnetic anisotropy by way of studying the in-plane and perpendicular magnetism. Examining different Co/Pt multilayers made using different V_{EH} (ion energies), we have ascertained that 1.2 nm of Co is the minimum thickness required to establish perpendicular magnetic anisotropy (PMA) and that no intermixing of Co and Pt at their interface is necessary for PMA to occur. First-principles calculations, consistent with the analysis of electron-energy-loss spectrometry with near atomic resolution, indicate that PMA is due to hybridization of Co and Pt at the interface which results in a perpendicular magnetization axis being set in the Co layer due to a significant lowering of the interfacial anisotropy energy. These results point toward an interesting way to tune PMA in ultrathin Co/Pt multilayers.

DOI: 10.1103/PhysRevB.81.224412 PACS number(s): 75.30.Gw

I. INTRODUCTION

From a fundamental viewpoint, a precise control over the magnitude and type of anisotropy make multilayer (ML) thin films ideal for studying the formation of anisotropies in reduced geometries. Applications wise, in the recent past, thin-film MLs with perpendicular magnetic anisotropy (PMA) drew a great deal of attention due to their use in vertical magneto-optical recording.[1,2] More recently, thin-film MLs with PMA have been used to improve the density, stability, and reliability of spin valves and magnetic tunnel junctions.[3–5] PMA thin films are also promising candidates in the design of spintronic-based devices[6] and are used in systems that exploit perpendicular exchange bias,[7,8] where PMA-based multilayer thin films are used to facilitate control of the magnetic orientation in devices. Clearly, tailoring the PMA of thin-film multilayers is likely to be a requirement for further technological developments and underpinning that is a comprehensive understanding its origins.

Multilayers of Co/Pt and Co/Pd are known to exhibit PMA.[9,10] Specifically, Co/Pt multilayer systems that exhibit parallel and perpendicular anisotropies simultaneously have been an area of significant interest recently with the observation of a spin reorientation transition to a "cone state"[1,2,9–15] whose origin is under debate currently. In addition, recently PMA in [Pt/Co] multilayer systems has been shown to become altered significantly when ultrathin Pt spacers between the [Pt/Co] ML and the antiferromagnetic (AF) layer is used, or different combinations of layer thickness,[16] and by varying the Co thickness in the CoO[Co/Pt] MLs.[17] It has been proposed that PMA in ultrathin Co/Pt MLs (where the Co layer thickness is around 1 nm) is either from interfacial intermixing of Co and Pt, or from an interfacial magnetic anisotropy present without intermixing.[10,18,19] The heat of mixing and interfacial energy should be the main contributors to the free energy of elemental intermixing that occurs in the ultrathin-film systems.[20] A negative heat of mixing (−5.27 eV/Co-Pt atomic pair[21]) has been determined by constructing the alloy from Wigner-Seitz atomic cells taken from the pure metallic elements. From this, the magnetic spins can be related to the microstructure through spin-orbit coupling. Since the bonding energy's magnitude is usually much higher than the magnetic coupling energy,[22] it should be possible to tune the PMA in ultrathin Co/Pt films by varying the interfacial energy of Co/Pt. In this paper, we demonstrate that this indeed is possible by modulating the preferred orientation of NiO sublayer with a dual ion-beam deposition technique. The NiO layer under the $[Pt/Co]_4$ multilayers was chosen because the preferred orientation of NiO can be adjusted[23,24] to modulate the interfacial energies between the NiO and Co layers, which will in turn affect the atomic arrangements between the Co and Pt layers. Our results on Co/Pt coupled to the antiferromagnet NiO provide a quantitative description of PMA's origins and help elucidate the thickness dependence of the multilayers on PMA.

II. EXPERIMENTAL METHODS

$[Pt/Co]_4/NiO$ multilayers on a SiO_2 substrate were prepared using a dual ion-beam deposition technique (DIBT).[23,25,26] The DIBT system consisted of a Kaufman deposition source and an End-Hall assisted source. The End-Hall source was used before deposition to bombard the substrate and to make the 20-nm-thick NiO layer by using a 16% oxygen-to-argon mixture of ions with a pure Ni target. During NiO deposition, End-Hall voltages (V_{EH}) of 100 and 140 V were used to provide different bombardment energies.

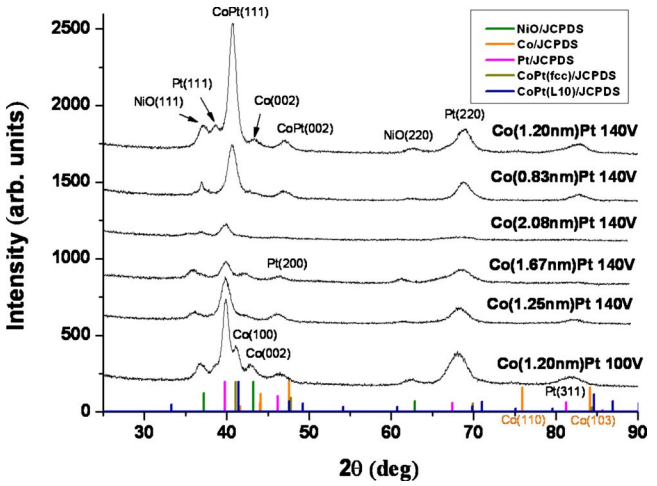

FIG. 1. (Color online) X-ray diffraction patterns of $[Pt/Co]_4/NiO$ multilayer systems with different Co thickness and V_{EH} for incident grazing angle of 1°. The line profiles from the JCPDS—International Centre for Diffraction Data for x-ray powder results are included for comparison.

The Kaufman source was used to focus an argon-ion beam onto a Pt or Co target. Each multilayer film had a 3-nm-thick Pt layer together with a Co layer that ranged between 0.8 and 2.0 nm in thickness. The series of Co and Pt layers was capped with Pt for a protective layer to prevent oxidation. No external field was applied during deposition.

The crystal structures of the $[Pt/Co]_4/NiO$ multilayers were characterized with x-ray diffraction (XRD) at a grazing angle of 1°. A JEOL (JEM-2100F) transmission electron microscope (TEM) equipped with electron-energy-loss spectroscopy (EELS) operating at 200 kV was used for microstructural and electronic analyses. In-plane and perpendicular hysteresis loops of the multilayers were measured at room temperature with a commercial vibrating sample magnetometer after being field cooled from above 350 K in 20 kOe. The temperature dependence of the magnetization was determined with a superconducting quantum interference device magnetometer (Quantum Design MPMS), where the zero-field-cooled (ZFC) measurements were performed with field profiling about the sample position and field canceling trim coils to nullify any external fields after the sample space had been field provided. The first-principles calculations were performed using the Vienna *ab initio* simulation package (VASP) to obtain the electronic structures and interfacial energies.[27,28] The supercells used in the calculations, which include the interface between Co and Pt,[29] were constructed from the analyses of high-resolution TEM (HRTEM) images.

III. RESULTS AND DISCUSSION

XRD patterns of the films shown in Fig. 1 indicated a mixed CoPt phase (having a disordered fcc structure, $Fm3m$) when the Co thickness was less than or equal to 1.20 nm and $V_{EH}=140$ V. These results were in agreement with previous work[10] that showed a chemically mixed interface was responsible for PMA when the Co layer thickness was less than 1.4 nm. A Co/Pt multilayer scheme without the Co-Pt mixed composition interface was made with a 1.2 nm Co thickness using $V_{EH}=100$ V (Fig. 1) where the lower argon-ion energy (V_{EH}) prevented intermixing. It is known that Co-Pt alloys exhibit a negative heat of mixing (−5.27 eV/Co-Pt atomic pair) (Ref. 21) which is likely responsible for the creation of the mixed Co/Pt phase in the multilayer structure.

At 300 K, parallel (in plane) and perpendicular (out of plane) M vs H measurements of the films with different Co thicknesses deposited using $V_{EH}=140$ V identified very little change in the in-plane anisotropy as $H_{c\|}$ was essentially independent of Co thickness (shown in the top-left panel of Fig. 2) while the in-plane unidirectional anisotropy required more than ~1.2 nm of Co for the NiO to couple to (bottom-left panel of Fig. 2) so that $H_{ex\|}>0$ with its positive value consistent with ferromagnetic (FM)-like interface coupling.[7] Interestingly, the out-of-plane anisotropy described by $H_{c\perp}$ showed a marked Co thickness dependence when more than ~1.2 nm of Co was deposited, and an increase in the perpendicular exchange coupling $H_{ex\perp}$ (similar to that observed in $H_{ex\|}$ for >1.2 nm Co) was observed (right panels of Fig. 2). The changes in H_c and H_{ex} between Co thicknesses of ~1.2 and ~1.7 nm indicated a change in the interfacial magnetic spin configuration between the Co and the NiO with concomitant interfacial mixing of Co, Ni, and O.[25] To investigate this change in magnetism at the AF/FM interface and its effects on the parallel and perpendicular anisotropies, removing possible thickness effects is desired (since the exchange energies associated with H_{ex} are affected by the AF and FM's thicknesses[7]). Previous work has shown that thickness effects can be mirrored by using different V_{EH} voltages used during the Co deposition.[25] In addition, the lower V_{EH} precluded any interfacial intermixing (see above). By using $V_{EH}=100$ V during the 1.2 nm Co thickness deposition, we retain the same basic parallel anisotropy magnetism (■ for $H_{c\|}$ and $H_{ex\|}$ in Fig. 2) and induce similar perpendicular anisotropy components as the 1.7 nm Co-based film (■ for $H_{c\perp}$ in Fig. 2) and a changed T_B for $H_{ex\perp}$.

Figure 3 shows the results of ZFC and FC in-plane magnetization ($H_{\|}$) as a function of temperature for the $[Pt/Co(1.2\ nm)]_4/NiO$ $V_{EH}=100$ and 140 V films. $M_{ZFC}(T)$ for the $V_{EH}=100$ V film was essentially constant with warming from 10 to 400 K, and the subsequent $M_{FC}(T)$ gradually increased with cooling as more CoPt at the interface with the NiO (detailed below) aligned with the 100 Oe field. These results are consistent with the measurements occurring below the T_N of NiO with no evidence of a spin reorientation of CoPt moments with the NiO interfacial moments via exchange coupling shown clearly by the lack of convergence between $M_{ZFC}(T)$ and $M_{FC}(T)$. However, there is a broad "hump" in $M_{ZFC}(T)$ between 150 and 225 K, which may be an indication of a weak change in the spin orientation between the NiO and Co layer. By contrast, for the $V_{EH}=140$ V film, above 350 K there was clear divergence between $M_{ZFC}(T)$ and $M_{FC}(T)$ at around 370 K, which was from a spin reorientation into the measuring field of the CoPt crystallites coupled to the NiO, behavior which provided a strong indication of a different anisotropy present in the $V_{EH}=140$ V film. Further evidence of the different magnetism between the films was provided by the in-plane (‖)

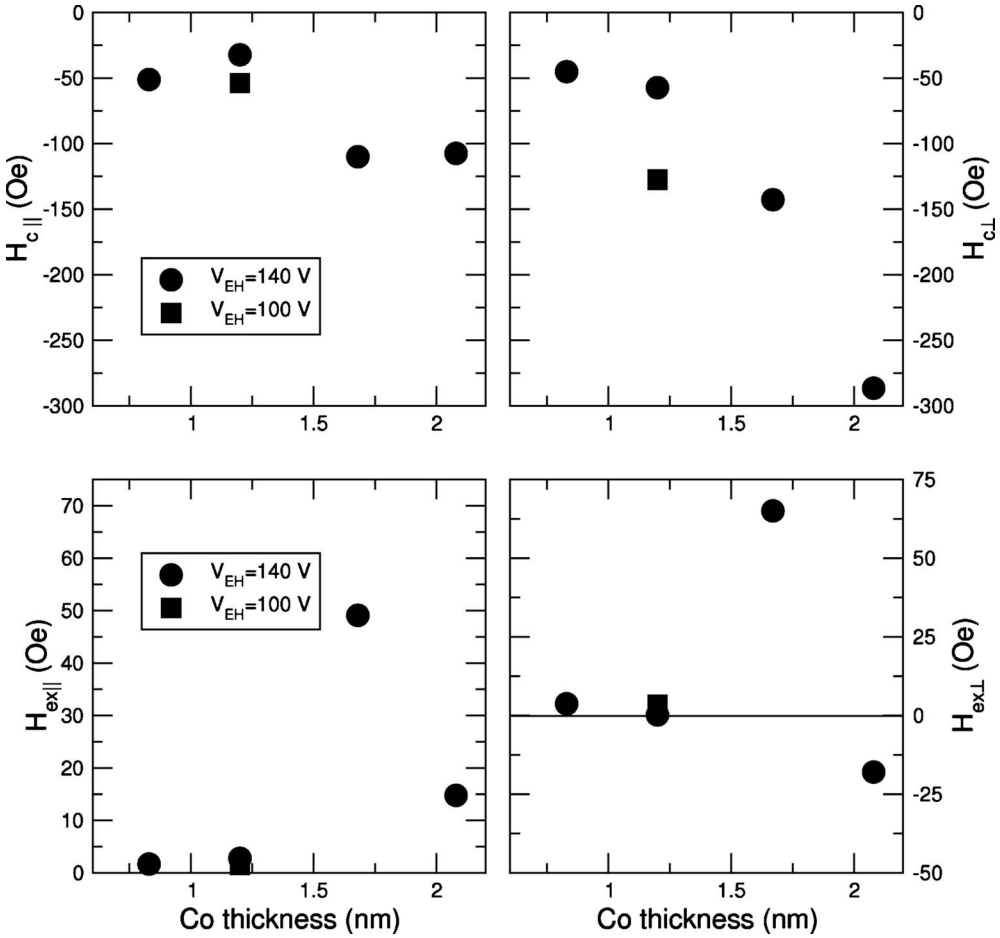

FIG. 2. Co thickness dependence of the parallel and perpendicular coercivities ($H_{c\|}$ and $H_{c\perp}$) and exchange bias fields ($H_{ex\|}$ and $H_{ex\perp}$) at 300 K.

and perpendicular ($\perp$) hysteresis loops presented in Figs. 4 and 5. PMA components are present in both V_{EH}=100 V (at 170 K) and V_{EH}=140 V (at 298 K). As hinted at by the $M_{ZFC}(T)$ results for the V_{EH}=100 V, a weaker PMA was present, and thus its effects were not observed at 298 K in the hysteresis loop. The origins of the weaker PMA in the V_{EH}=100 V compared to the V_{EH}=140 V film was due to its different microstructure. Plane-view TEM images (not shown) revealed an average CoPt phase crystallite diameter of 6.3 nm for V_{EH}=140 V and 4.7 nm for V_{EH}=100 V. These results are consistent with Scherrer analysis of the XRD diffraction peaks[30] with 6.5 nm for V_{EH}=140 V and 4.4 nm for V_{EH}=100 V. In addition, we find that the largest volume of grains (from both cross-section and plane-view TEM analyses) to be about 390 nm^3 which allows us to estimate the temperature that PMA will be observed using the phenomenological criteria[31] $K_uV/k_BT \geq 60$, where $K_u \sim 4.5\times10^6$ erg/cm^3 is the magnetocrystalline anisotropy constant of the Co,[32] V is the average crystallite volume, k_B is Boltzmann's constant, and T is the temperature. Estimates of the onset temperature of PMA identify that at 170 K PMA should be present in the V_{EH}=100 V film and absent at 300 K, and present above room temperature in the V_{EH}=140 V film, in good agreement with our measurements.

In addition, since there is always competition, or frustration, between the shape and magnetocrystalline anisotropies

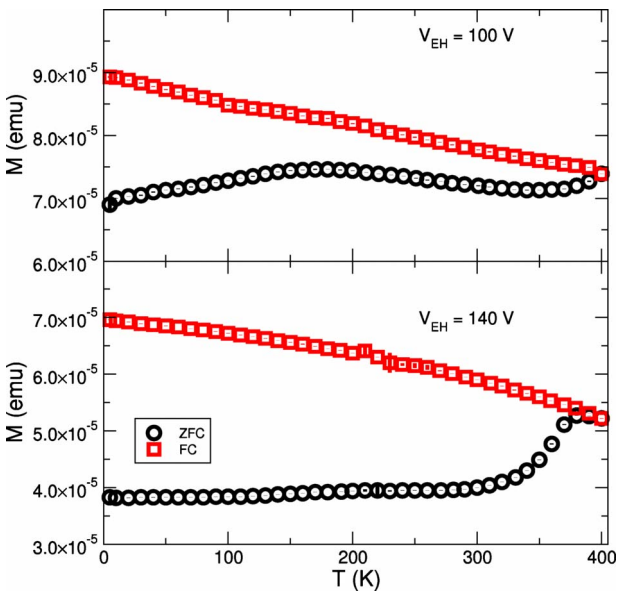

FIG. 3. (Color online) (Left) Temperature dependence of the zero-field-cooled and field-cooled magnetization in 100 Oe for the V_{EH}=100 and 140 V $[Co/Pt]_4/NiO$ films. (Right) Hysteresis loops for the films with multilayer scheme and intermixing indicates the existence of perpendicular magnetic anisotropy.

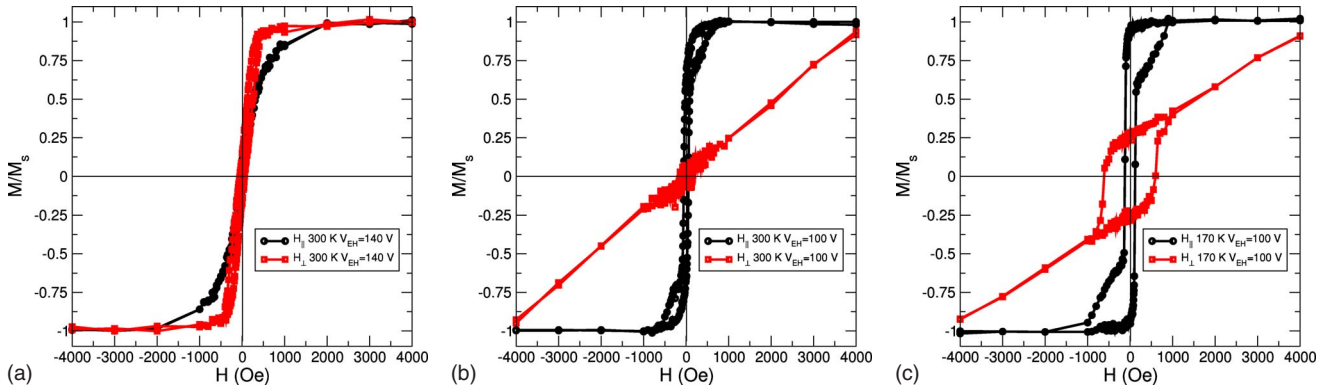

FIG. 4. (Color online) Hysteresis loops for the films with a multilayer scheme (V_{EH}=140 V) and intermixing (V_{EH}=100 V) show the existence of perpendicular magnetic anisotropy at different onset temperatures when the field is applied parallel ($H_{\|}$) and perpendicular ($H_{\perp}$) to the film plane.

that set the direction of the magnetization, a measure of the PMA strength can be described by a "effective anisotropy," K_{eff}, that is estimated from the area between the M vs $H_{\perp}$ and $H_{\|}$ loops via $K_{eff}=(1/V)\int_0^{H_{sat}}(M_{\perp}-M_{\|})dH$,[33] where H_{sat} is the field required to reach the film's saturation magnetization. The sign of K_{eff} is a measure of the preferred direction of the magnetization (e.g., $K_{eff}>0$ indicates a preference toward a perpendicular orientation and the usual in-plane orientation is denoted by large, negative values of K_{eff}). For the V_{EH}=100 V film with 1.2 nm Co thickness, $K_{eff}\sim 0$, consistent with a robust PMA component, while $K_{eff}\sim 0.5$ erg/cm^2 for the V_{EH}=140 V film, indicating an even stronger PMA.

Due to the nanocrystalline microstructure and intrinsic intracrystallite strains, neighboring diffraction peaks could have been broadened, overlapped or shifted, making it problematic to use XRD results to identify unequivocally the phases present in the films. Therefore, we turned to HRTEM to provide a more detailed microstructural picture of the films with the assistance of "multislice" simulations[34] that provided a first-principles image simulation of measured crystal structures, permitting a quantitative analysis of HRTEM results. The multislice method is the most commonly used method of calculating the electronic wave function emerging from a specimen under observation.[35] Using multislice, the atomic arrangements from the crystal structures of the Co and Pt layers (phases) around the interface can be identified in the films via detailed simulations of a crystal structure projected onto the HRTEM image patterns. This crystallographic information was used as the input of first-principles calculations to obtain the interfacial energy.

The interfacial energies as a function of the angles between the Co [002] and Pt [111] axes resulting from the above calculations are shown in Fig. 6(a). The numbers (1, 2, and 3) correspond to the interfacial regions in the HRTEM micrographs demarked for V_{EH}=140 V [Fig. 6(b)] and V_{EH}=100 V [Fig. 6(c)]. The corresponding interfacial atomic arrangements obtained from the multislice calculations are also included [Fig. 6(a)]. Our results indicated that the NiO ⟨111⟩ direction tended to be perpendicular to the film surface for the V_{EH}=100 V film [Fig. 6(c)]. Accounting for the symmetry and dimensional variation in the atomic arrangements,[20]

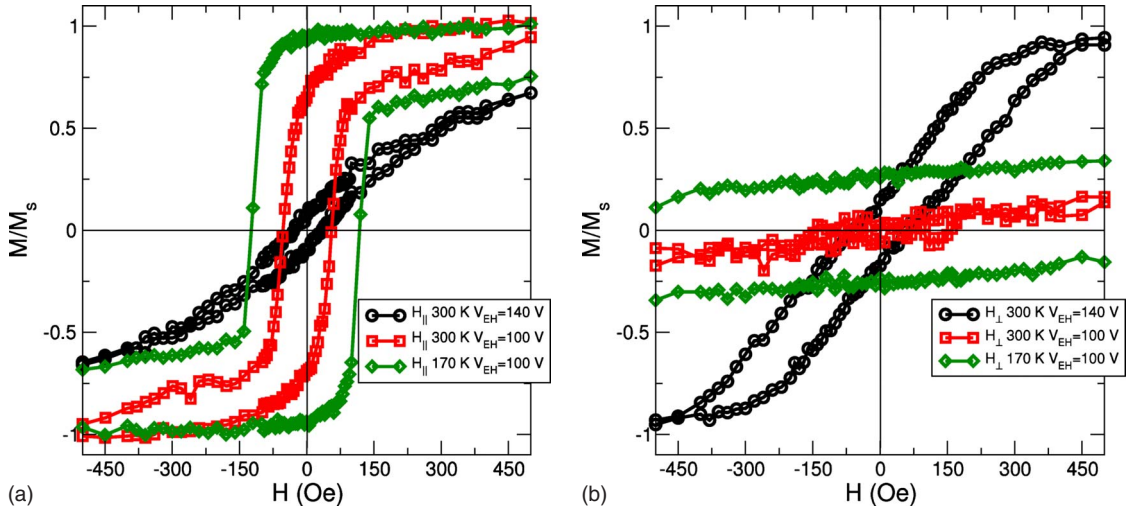

FIG. 5. (Color online) Low-field parts of the hysteresis loops with the fields parallel (top, $H_{\|}$) and perpendicular (bottom, $H_{\perp}$) to the film planes for the film with a multilayer scheme (V_{EH}=140 V) and the film with intermixing (V_{EH}=100 V) show the existence of perpendicular magnetic anisotropy at different onset temperatures.

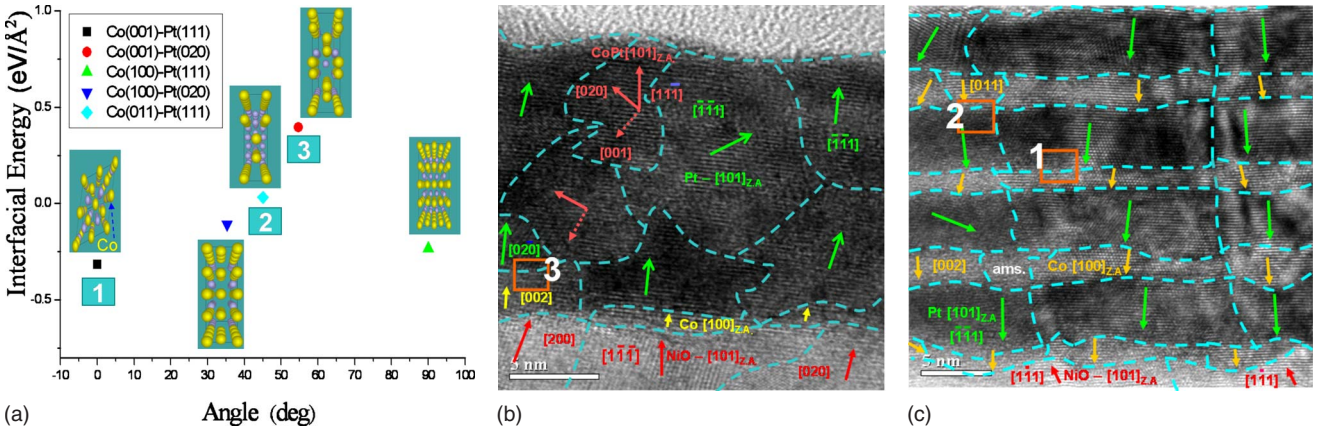

FIG. 6. (Color online) (a) Interfacial energies versus the angles between the Co [002] and Pt [111] axes, the numbers correspond to the marked regions of HRTEM micrographs shown in (b) and (c). (b) HRTEM for specimen with serious intermixing. (V_{EH}=140 V). (c) HRTEM for specimen with a multilayer scheme (V_{EH}=100 V). The arrows in (b) and (c) are the crystallographic orientations that due to the strong PMA should be coincident with the directions of magnetization (see text).

the calculations suggested that the Co basal plane preferred to be aligned with the NiO {111} and Pt {111} planes. These results indicated that the interfacial energy was lowered substantially for these arrangements [as shown in Fig. 6(a)]. Furthermore, comparing these results with first-principles theory of magnetocrystalline anisotropy in CoPt alloys[36] (from the atomic configuration) suggested that the Co/Pt multilayers with a perpendicular magnetic easy axis for Co might be present even in the V_{EH}=100 V film. As for the V_{EH} =140 V [Co/Pt]/NiO film, a mixed CoPt phase with a perpendicular ⟨111⟩ magnetic easy axis [Fig. 6(b)] was identified.[36] This phase formation was likely driven by the negative heat of mixing and much higher interfacial energy caused by a different NiO layer texture induced by the increased Ar/O_2 ion bombardment energy used during NiO deposition. These results suggest that by adjusting the preferred orientations in the NiO we could modulate the interfacial energy between the Co and Pt layers and control the PMA.

Insight into the observed PMA and its effects on the magnetism in the V_{EH}=100 and 140 V films required detailed knowledge of the film microstructure and composition at and around the Co and Pt interfaces. We achieved this though calculated electronic structures from the first-principles analyses[37] of the Co/Pt MLs at the Co [002] parallel to Pt [111], illustrated in Fig. 7. The total density of states (DOS) of Co (number 3) and Pt (number 4) at their mutual interfaces was compared to those of the pure elemental counterparts (e.g., the elements in the middle of thin layers). We found that the total DOS are composed mainly of *d* orbitals. The strong Pt 5*d*-Co 3*d* hybridization across the interface can be associated with magnetic moments induced on Pt atoms, indicated by the asymmetry of distributions of ~0.2 μ_B/atom up and down spins (Fig. 7).[19,38,39] The average peak centers (that correspond to electronic energies) were observed clearly to move to lower energies, which established that the interface was significantly more stable (~0.5 eV/atom less). This trend provided unmistakable evidence that a strong 3*d*-5*d* hybridization localized at the Co/Pt interface helped set the Co [002] direction within the layer to orient perpendicular to the film surface, giving rise to PMA in addition to the effect of a strongly enhanced perpendicular Co orbital moment at the interface.[19] It should be noted that this type of strong hybridization cannot be identified for other crystallographic configurations.

In order to corroborate the results from the DOS calculations, EELS combined with HRTEM was used to obtain structural and electronic information at nearly the atomic scale.[40] Typical results of the *Z*-contrast image from TEM and EELS measurements are shown in Fig. 8. The *Z*-contrast image is from the high-angle annual dark field (HAADF).[41,42] In the HAADF, the high-energy electron must pass close to the nucleus in order to be scattered elastically or nearly elastically at a high angles. At a high angle, the scattering scales with the square of the atomic number (Z^2), as expected for Rutherford scattering from an unscreened nucleus.[42] Hence, elastically scattered electrons carry compositional information through this *Z* dependence of the scattering cross section. Since the *Z* of Pt is much higher than that of Co, the Pt layer in the *Z*-contrast image is much

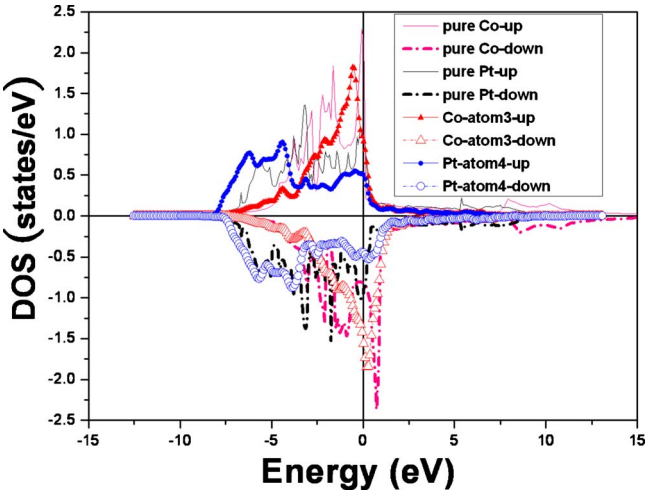

FIG. 7. (Color online) The hybridization between Co and Pt occurring at the interface.

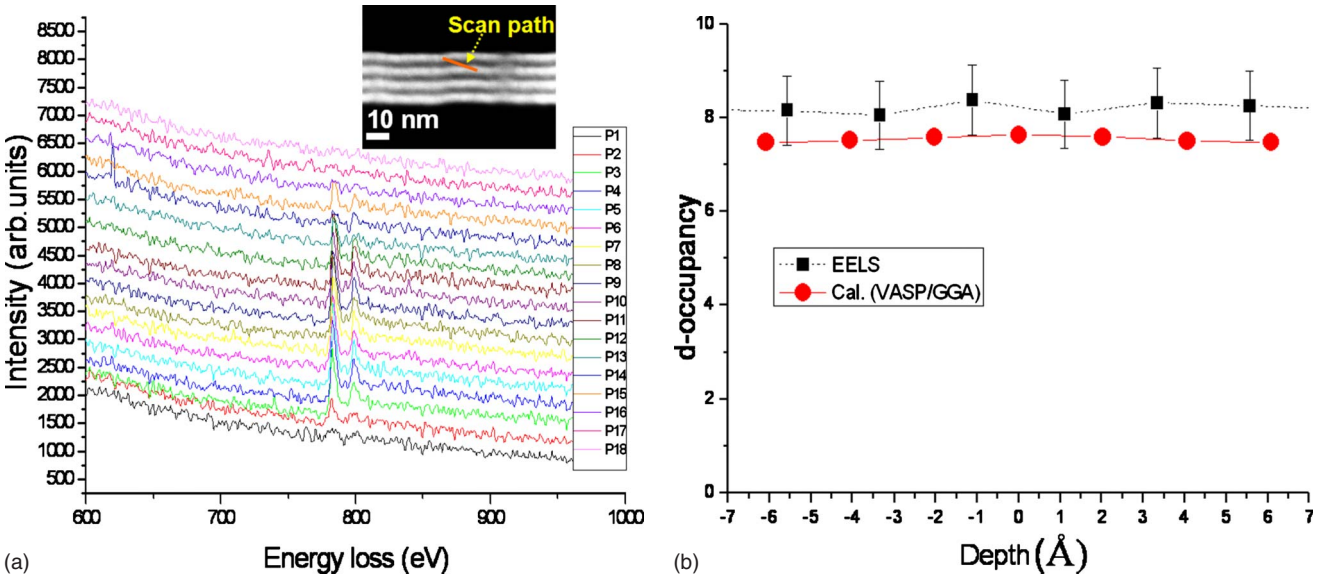

FIG. 8. (Color online) Top: EELS spectra recorded point by point across the Co/Pt multilayer Co layers as indicated in the insert of HAADF micrograph. Bottom: the *d* occupancies from both normalized white-line intensity and simulated results of first-principles calculations within Co layer (the center of Co layer was defined as zero depth).

brighter than that of Co layer. The scan path shown in Fig. 8 (P1–P18 that corresponds to approximately 1 nm steps as shown in the inset identifying the scan path) is where the spectra of nearly atomic EELS were acquired evenly column by column along the scan path (P1–P18) with a 5 Å beam-spot size.[40] With these measurements, we were able to examine the $L_{2,3}$ absorption edges within the layers. In general, the most useful features for characterization purposes of transition metals and related oxides are the distinctive peaks known as "white lines" that are found at the onset of the $L_{2,3}$ absorption edges, due to the excitation of $2p_{1/2}$ or $2p_{3/3}$ core electrons in an atom to the unoccupied *d*-like states near the Fermi level.[24,43,44] The white lines acquired by EELS provide information that is local to a given atomic species.[45–47] Therefore, we were able to ascertain local *d* occupancy within the Co layer both from the EELS as shown in Fig. 8 and compare with DOS of the first-principles calculations. The *d* occupancy from DOS was determined from the *d* orbitals by calculating the area up to Fermi level and then normalizing to the total area. For the *d*-occupancy analysis of EELS, *d*-shell holes of a transition metal can be obtained by isolating white lines from the background intensity after deconvolution so as to determine the $L_{2,3}$ intensity.[24,43,44] In addition, by correct normalization of the single-scattering distribution and evaluation of matrix element,[24,43,44,48] effects such as variations in film thickness and possible changes in oxidation state are incorporated into the analysis technique. Results of the 3*d* occupancy of Co within the layer by EELS are also shown in Fig. 8 and compared with results from first-principles calculations. Excellent agreement between the EELS and first-principles analyses was observed, confirming our interpretation of the atomic configurations at the interfaces in the multilayers and their relationship to the onset of PMA and its magnetism.

IV. CONCLUSIONS

In summary, it was demonstrated in this investigation that both the mixed CoPt phase and ultrathin Co layer with perpendicular easy axes can be responsible for PMA, independently. The occurrence of the mixed CoPt phases is due to the negative heat of mixing and relatively unstable interfacial structure when the thickness of Co is 1.2 nm or less. The MLs with PMA can be prepared by aligning the Co basal plane with both NiO {111} and Pt {111} planes in the film plane through tuned ion bombardment via the DIBT method. The relatively stable interfacial structure is closely related to the strong Pt 5*d*–Co 3*d* hybridization across the interface. Furthermore, tailoring the texturing of the sublayer by DIBT provides a valuable tool to engineer PMA in ultrathin Co/Pt multilayers. Finally, we have ascertained that while a mixed CoPt phase at the Co/Pt does indeed result in PMA, contrary to the previous understanding of PMA's origins[9,10,12] it is not a necessary requirement, and that by appropriate tuning of the ferromagnetic/antiferromagnetic interface (here Co with NiO), PMA is possible even when a uniform multilayer scheme is present with no interfacial intermixing.

ACKNOWLEDGMENTS

Research was supported by the National Science Council of Taiwan, by the Natural Sciences and Engineering Research Council of Canada, and the Canada Foundation for Innovation. We are also grateful to the National Center for High-Performance Computing of Taiwan for computer time and facilities.

[1] M. Johnson, P. Bloemen, F. den Broedery, and J. J. de Vries, Rep. Prog. Phys. **59**, 1409 (1996).
[2] P. Gambardella *et al.*, Science **300**, 1130 (2003).
[3] N. Nishimura, T. Hirai, A. Koganei, T. Ikeda, K. Okano, Y. Sekiguchi, and Y. Osada, J. Appl. Phys. **91**, 5246 (2002).
[4] V. Skumryev, S. Stoyanov, Y. Zhang, G. Hadjipanayis, D. Givord, and J. Nogués, Nature (London) **423**, 850 (2003).
[5] J. Eisenmenger and I. K. Schuller, Nature (London) **2**, 437 (2003).
[6] S. Mangin, D. Ravelosona, J. A. Katine, M. J. Carey, B. D. Terris, and E. E. Fullerton, Nature Mater. **5**, 210 (2006).
[7] J. Nogués and I. K. Schuller, J. Magn. Magn. Mater. **192**, 203 (1999).
[8] S. Maat, K. Takano, S. S. P. Parkin, and E. E. Fullerton, Phys. Rev. Lett. **87**, 087202 (2001).
[9] P. F. Carcia, A. D. Meinhardt, and A. Suna, Appl. Phys. Lett. **47**, 178 (1985).
[10] P. F. Carcia, J. Appl. Phys. **63**, 5066 (1988).
[11] S. Hashimoto, Y. Ochiai, and K. Aso, J. Appl. Phys. **66**, 4909 (1989).
[12] W. B. Zeper, F. J. Greidanus, and P. F. Carcia, IEEE Trans. Magn. **25**, 3764 (1989).
[13] C. J. Lin, G. L. Gorman, C. H. Lee, R. F. C. Farrow, E. E. Marinero, H. Do, H. Notarys, and C. J. Chien, J. Magn. Magn. Mater. **93**, 194 (1991).
[14] D. Weller, R. F. Farrow, R. F. Marks, G. R. Harp, H. Notarys, and G. Gorman, *Magnetic Ultrathin Films: Multilayers and Surfaces, Interfaces and Characterization*, MRS Symposia Proceedings No. 313 (Materials Research Society, Pittsburgh, 1993), p. 791.
[15] R. Frömter, H. Stillrich, C. Menk, and H. P. Oepen, Phys. Rev. Lett. **100**, 207202 (2008).
[16] J. Sort, V. Baltz, F. Garcia, B. Rodmacq, and B. Dieny, Phys. Rev. B **71**, 054411 (2005).
[17] E. Shipton, K. Chan, T. Hauet, O. Hellwig, and E. Fullerton, Appl. Phys. Lett. **95**, 132509 (2009).
[18] H. Nemoto and Y. Hosoe, J. Appl. Phys. **97**, 10J109 (2005).
[19] N. Nakajima, T. Koide, T. Shidara, H. Miyauchi, H. Fukutani, A. Fujimori, K. Iio, T. Katayama, M. Nyvlt, and Y. Suzuki, Phys. Rev. Lett. **81**, 5229 (1998).
[20] D. Porter and K. Easterling, *Phase Transformations in Metal and Alloys* (Chapman and Hall, London, 1992).
[21] A. Miedema, F. de Boer, and R. Boom, CALPHAD: Comput. Coupling Phase Diagrams Thermochem. **1**, 341 (1977).
[22] C. Kittel, *Introduction to Solid State Physics*, 8th ed. (Wiley, Berlin, 2005).
[23] C.-H. Su, S.-C. Lo, K.-W. Lin, J. van Lierop, and H. Ouyang, J. Appl. Phys. **105**, 033904 (2009).
[24] H. Ouyang, K.-W. Lin, C.-C. Liu, S.-C. Lo, Y.-M. Tzeng, Z.-Y. Guo, and J. van Lierop, Phys. Rev. Lett. **98**, 097204 (2007).
[25] C.-H. Su, S.-C. Lo, S.-H. Chiou, K.-W. Lin, W. Ouyang, and H. Ouyang, Electrochem. Solid-State Lett. **12**, K1 (2009).
[26] C.-H. Su, S.-C. Lo, J. van Lierop, K.-W. Lin, and H. Ouyang, J. Appl. Phys. **105**, 07C316 (2009).
[27] G. Kresse and J. Hafner, Phys. Rev. B **47**, 558 (1993).
[28] G. Kresse and J. Furthmüller, Phys. Rev. B **54**, 11169 (1996).
[29] M. Payne, M. Teter, D. Allen, T. Arias, and J. Joannopoulos, Rev. Mod. Phys. **64**, 1045 (1992).
[30] N. Das, P. Mondal, and D. Bhattacharya, Phys. Rev. B **74**, 014410 (2006).
[31] P.-L. Lu and S. H. Charap, IEEE Trans. Magn. **30**, 4230 (1994).
[32] W. Yang, D. N. Lambeth, and D. E. Laughlin, J. Appl. Phys. **87**, 6884 (2000).
[33] C. H. Lee, H. He, F. J. Lamelas, W. Vavra, C. Uher, and R. Clarke, Phys. Rev. B **42**, 1066 (1990).
[34] E. J. Kirkland, *Advanced Computing in Electron Microscopy* (Plenum, New York, 1998).
[35] P. G. Self, M. A. O'Keefe, P. R. Buseck, and A. E. C. Spargo, Ultramicroscopy **11**, 35 (1983).
[36] S. S. A. Razee, J. B. Staunton, and F. J. Pinski, Phys. Rev. B **56**, 8082 (1997).
[37] H. Ouyang, H.-H. Chiou, Y.-C. S. Wu, J.-H. Cheng, and W. Ouyang, J. Appl. Phys. **102**, 013710 (2007).
[38] P. Ravindran, A. Kjekshus, H. Fjellvåg, P. James, L. Nordström, B. Johansson, and O. Eriksson, Phys. Rev. B **63**, 144409 (2001).
[39] J. Geissler, E. Goering, M. Justen, F. Weigand, G. Schütz, J. Langer, D. Schmitz, H. Maletta, and R. Mattheis, Phys. Rev. B **65**, 020405(R) (2001).
[40] S. J. Pennycook, M. Varela, A. R. Lupini, M. P. Oxley, and M. F. Chisholm, J. Electron Microsc. **58**, 87 (2009).
[41] B. Fultz and J. M. Howe, *Transmission Electron Microscopy and Diffractometry of Materials*, 3rd ed. (Springer, Berlin, 2008).
[42] S. Pennycook, Adv. Imaging Electron Phys. **123**, 173 (2002).
[43] D. H. Pearson, C. C. Ahn, and B. Fultz, Phys. Rev. B **47**, 8471 (1993).
[44] J. Graetz, C. C. Ahn, H. Ouyang, P. Rez, and B. Fultz, Phys. Rev. B **69**, 235103 (2004).
[45] P. Rez, *Transmission Electron Energy Loss Spectroscopy in Materials Science* (TMS, Warrendale, 1992), p. 122.
[46] D. Muller and J. Silcox, Ultramicroscopy **59**, 195 (1995).
[47] R. F. Egerton, Ultramicroscopy **107**, 575 (2007).
[48] R. F. Egerton, *Electron Energy Loss Spectrometry in the Electron Microscope* (Plenum, New York, 1996).